Small-Signal Analysis and Control Design of Isolated Power Supplies With Optocoupler Feedback

Yuri Panov and Milan M. Jovanović, *Fellow, IEEE*

***Abstract*—Optocouplers are widely used in isolated power supplies to transfer the feedback signal from the secondary to the primary side. In many power supplies, the feedback amplifier is supplied from the output voltage that creates additional feedback path which should be taken into account in the control design. The paper presents a detailed analysis and control design for each of the two possible feedback loops that can be identified. In addition, dynamic limitations of the TL431 shunt regulator and of the optocoupler are discussed. Practical guidelines for the error amplifier design and a design example are presented for both voltage-mode and current-mode controls.**

***Index Terms*—Feedback loop, isolated power supply, optocoupler.**

I. Introduction

GENERALLY, offline and telecom power supplies require the galvanic isolation between a relatively high input voltage and low output voltages. The most widely used devices to transfer signals across the isolation boundary are pulse transformers and optocouplers. The typical isolated power supply with the primary-side PWM control and optocoupler isolation is shown in Fig. 1. The feedback circuit shown in Fig. 1 is very popular in low-power/low-cost power supplies which usually do not have the standby converter to supply the TL431 shunt regulator but use output voltage $\mathrm{V_O}$ for this purpose. It is well known [1]–[7] that by supplying the TL431 from the output voltage an additional feedback path is introduced. Therefore, in the control circuit in Fig. 1, two loop gains which correspond to breaking the loop at locations A and B can be considered. The existence of two loops immediately raises the question which loop gain should be analyzed and measured in order to meet the power supply stability and dynamic response specifications. From the general control theory, each loop gain of the entire control system yields the same characteristic polynomial [8] and, therefore, reveals the system stability. However, depending on the chosen loop gain, error amplifier (EA) design is different which leads to different stability margins and different dynamic performance.

The purpose of the paper is to present comparative analysis of loop gains corresponding to breaking the loop at points A and B and to provide design guidelines based on each of these two loops. Section II of the paper provides general loop gain analysis and interpretation. Section III presents the comparative analysis of loop gains T_A and T_B for the power supplies with the voltage-mode and the current-mode controls. Section III also discusses design limitations of the TL431 shunt regulator and of the optocoupler circuit. Sections IV and V present the design example and experimental results, respectively, whereas Section VI summarizes the paper.

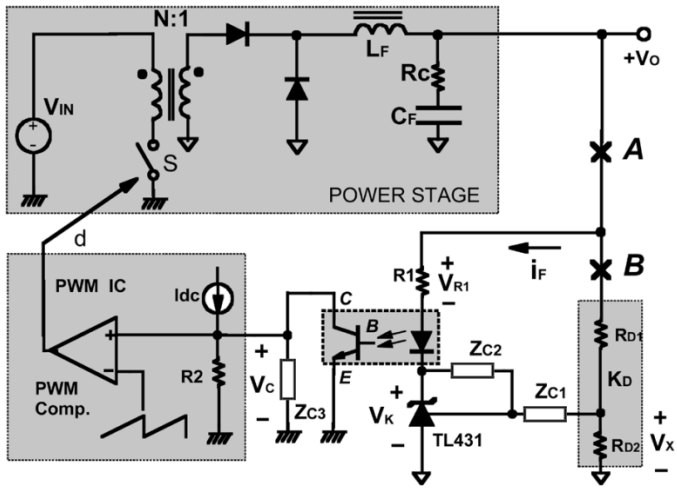

Fig. 1. Simplified circuit diagram of isolated power supply with optocoupler feedback.

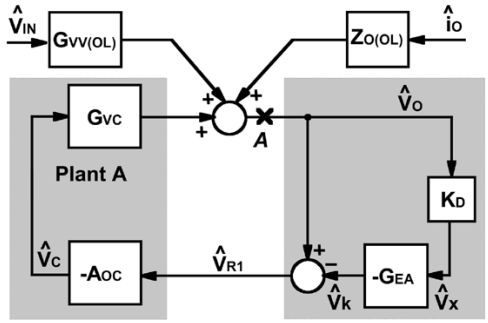

Fig. 2. Small-signal block diagram corresponding to breaking the loop at point A.

II. Loop Gain Analysis and Interpretation

A. Loop Gain T_A

The small-signal block diagram corresponding to breaking the loop at point A is shown in Fig. 2. Fig. 2 contains following blocks: K_D—output voltage divider gain, $G_{EA} = -\hat{V}_K/\hat{V}_X$—error amplifier transfer function, $A_{OC} = \hat{V}_C/\hat{V}_{R1}$—optocoupler circuit gain, $G_{VC} = \hat{V}_O/\hat{V}_C$—control-to-output transfer function, $G_{VV(OL)} = \hat{V}_O/\hat{V}_{IN}$—open-loop

Manuscript received April 21, 2004; revised December 14, 2004. The paper was presented at APEC-2004, Anaheim, CA, February 2004. Recommended by Associate Editor C. K. Tse.

The authors are with the Power Electronics Laboratory, Delta Products Corporation, Research Triangle Park, NC 27709 USA (e-mail: ypanov@deltartp.com).

Digital Object Identifier 10.1109/TPEL.2005.850926

audio susceptibility, $Z_{O(OL)} = \hat{V}_O/\hat{i}_O$—open-loop output impedance.

At point A in Fig. 2, the feedback signal is confined to a single path. Loop gain T_A, corresponding to breaking the loop at point A, is derived as

$$T_A = A_{OC} \cdot G_{VC} \cdot (1 + K_D \cdot G_{EA}). \tag{1}$$

The plant transfer function that provides the basis for the EA design is defined as

$$G_{PL(A)} = A_{OC} \cdot G_{VC}. \tag{2}$$

It should be noted that the EA is not connected in series with the plant and zeroes of $G_{\rm EA}$ generally do not translate into the same zeroes of the loop gain T_A. However, in many cases, $K_{\rm D} \cdot G_{\rm EA} \gg 1$ within the loop bandwidth and loop gain T_A can be written as

$$T_A \approx G_{PL(A)} \cdot K_D \cdot G_{EA}. \tag{3}$$

For loop gain T_A given in (3), the EA design procedure does not differ from that for the implementation where the optocoupler is supplied from the fixed voltage. If condition $K_{\rm D} \cdot G_{\rm EA} \gg 1$ is not satisfied within the loop bandwidth, the relationship between the zeroes of terms $K_{\rm D} \cdot G_{\rm EA}$ and $[1 + K_{\rm D} \cdot G_{\rm EA}]$ can be very complex, particularly, when the EA transfer function has more than two poles. To simplify the EA design in this case, it is recommended to keep the order of the EA transfer function not higher than two, but to add necessary poles and zeroes by connecting compensation network Z_{C3} on the primary side, as shown in Fig. 1. There is one more reason to connect compensation network Z_{C3} on the primary side. Term $[1 + K_D \cdot G_{EA}]$ in (1) has the slope of 0 dB/dec at high frequencies. To attenuate the switching noise at high frequencies, it is desirable to add the primary-side pole at the crossover frequency of term $K_D \cdot G_{EA}$.

It is important to find the relationship between loop gain T_A and the converter frequency-domain response to line and load variations. To simplify the analysis, it is assumed that the converter operates with the voltage-mode control. The closed-loop audio susceptibility $G_{VV(CL)}$ and output impedance $Z_{O(CL)}$ are derived from the block diagram in Fig. 2 as

$$G_{VV(CL)} = \frac{G_{VV(OL)}}{1 + T_A} \tag{4}$$

and

$$Z_{O(CL)} = \frac{Z_{O(OL)}}{1 + T_A}. \tag{5}$$

Relationships (4) and (5) are straightforward and imply that it is desirable to maximize loop gain T_A in order to achieve the best rejection of line and load disturbances.

B. Loop Gain T_B

The small-signal block diagram corresponding to breaking the loop at point B is shown in Fig. 3. After opening the loop at point B, the feedback signal propagates through resistor R_1 and affects LED current $\rm i_F$ in Fig. 1. Observation of the block diagram in Fig. 3 shows that, after breaking the loop at location B, the inner control loop still exists with the gain of

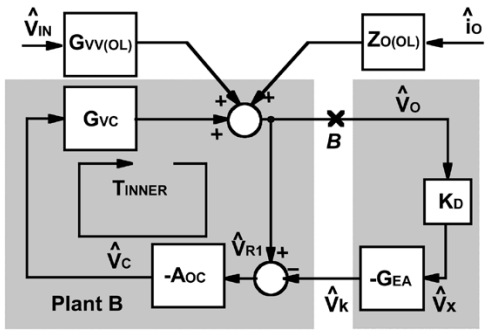

Fig. 3. Small-signal block diagram corresponding to breaking the loop at point B.

$$T_{INNER} = A_{OC} \cdot G_{VC}. \tag{6}$$

Loop gain $T_{\rm B}$, corresponding to breaking at the loop point B in Fig. 3, is derived as

$$\begin{aligned} T_B &= K_D \cdot G_{EA} \cdot \frac{A_{OC} \cdot G_{VC}}{1 + A_{OC} \cdot G_{VC}} \\ &= K_D \cdot G_{EA} \cdot \frac{T_{INNER}}{1 + T_{INNER}}. \end{aligned} \tag{7}$$

Generally, because loop B contains the inner feedback loop, the design of loop gain $T_{\rm B}$ is a two-step procedure. Namely, prior to loop gain $T_{\rm B}$ analysis, $T_{\rm INNER}$ gain must be examined for stability. The inner loop gain is relatively low because it does not contain the high-gain EA and its stability rarely becomes an issue in practice. It should be noted that $T_{\rm INNER}$ can be compensated by connecting network Z_{C3} on the primary side, as shown in Fig. 1, so that the design of loop gain $T_{\rm B}$ can be further optimized. The analysis and implementation of the inner loop compensation was presented in [9] in the context of the magamp control. In fact, the control of the isolated power supply with optocoupler supplied from the output voltage is similar to the magamp control where the magamp reset circuit is supplied from the output voltage [9], [10].

Equations (1), (6), and (7) are used to derive the relationship between T_A and $T_{\rm B}$

$$T_A = T_{INNER} + (1 + T_{INNER}) \cdot T_B. \tag{8}$$

The last equation indicates that there is no unique relationship between T_A and $T_{\rm B}$, unless $T_{\rm INNER}$ is known. The plant transfer function that provides the basis for the EA design is defined as

$$\begin{aligned} G_{PL(B)} &= \frac{T_{INNER}}{1 + T_{INNER}} = \frac{A_{OC} \cdot G_{VC}}{1 + A_{OC} \cdot G_{VC}} \\ &= \frac{G_{PL(A)}}{1 + G_{PL(A)}}. \end{aligned} \tag{9}$$

Comparison of (2) and (9) reveals that the poles of plant transfer function $G_{PL(B)}$ are different from those of plant transfer function $G_{PL(A)}$. Namely, at low frequencies, where $T_{INNER} \gg 1$, transfer function $G_{PL(B)} \approx 1$. At high frequencies, where $T_{INNER} \ll 1$, transfer function $G_{PL(B)} \approx G_{PL(A)}$. The poles of $G_{\rm PL(B)}$ are actually shifted to higher frequencies with respect

to those of $G_{\mathrm{PL}(A)}$ [9], [10]. Hence, the compensator poles and zeroes are selected differently depending on which loop gain, T_A or T_{B}, is used for the design.

Loop gain T_{B} can be written as

$$T_B = G_{PL(B)} \cdot K_D \cdot G_{EA}. \tag{10}$$

From the block diagram in Fig. 3, the relationship between loop gain T_{B} and closed-loop audio susceptibility $G_{\mathrm{VV(CL)}}$ and output impedance $Z_{\mathrm{O(CL)}}$ of the converter with the voltage-mode control is

$$G_{VV(CL)} = \frac{G_{VV(OL)}/(1+T_{INNER})}{1+T_B} = \frac{G_{VV(B)}}{1+T_B} \tag{11}$$

and

$$Z_{O(CL)} = \frac{Z_{O(OL)}/(1+T_{INNER})}{1+T_B} = \frac{Z_{CL(B)}}{1+T_B} \tag{12}$$

where

$$G_{VV(B)} = \frac{G_{VV(OL)}}{1+T_{INNER}} \tag{13}$$

and

$$Z_{CL(B)} = \frac{Z_{O(OL)}}{1+T_{INNER}}. \tag{14}$$

It should be noted that transfer functions $G_{VV(B)}$ and $Z_{CL(B)}$ given in (13) and (14) represent the audio susceptibility and output impedance of the converter with only the inner loop closed. Equations (11) and (12) indicate that for optimal rejection of line and load disturbances loop gain T_{B} as well as loop gain T_{INNER} should me maximized. Loop gain T_{INNER} can be maximized by compensating optocoupler circuit gain A_{OC}, whereas loop gain T_{B} can be optimized by compensating EA gain G_{EA}. However, placement of A_{OC} poles and zeroes at desired locations is not straightforward because their frequencies are dependent on the optocoupler circuit small-signal parameters, as it will be shown in Section III. Moreover, loop gain T_{INNER} affects plant transfer function $G_{\mathrm{PL(B)}}$ which is the basis for the EA design. Therefore, the design procedure for optimization of audio susceptibility and output impedance based on breaking the loop gain at point B is more complex than in the case of the design based on loop gain T_A. Moreover, as it is shown in Section III, the design procedure based on breaking the loop at point B is less accurate in determining power supply stability. Comparisons of EA designs based on loop gains T_A and T_{B} are presented in Section III.

III. Error Amplifier Design Considerations

A. Power Supplies With Voltage-Mode Control

Control-to-output transfer function G_{VC} of the forward converter in Fig. 1 in the case of the voltage-mode control and CCM operation is

$$G_{VC} = F_M \cdot G_{VD} \tag{15}$$

where

$$G_{VD} = \frac{V_{IN}}{N} \cdot \frac{1+s/\omega_{ZC}}{1+s/(\omega_0 \cdot Q)+s^2/\omega_0^2} \tag{16}$$

$$\omega_0 = \frac{1}{\sqrt{L_F \cdot C_F}} \tag{17}$$

$$Q = \frac{\sqrt{L_F \cdot C_F}}{L_F/R_L + R_C \cdot C_F} \tag{18}$$

$$\omega_{ZC} = \frac{1}{R_C \cdot C_F}. \tag{19}$$

R_L is the load resistance, and F_M is the gain of the pulse-width modulator (PWM) that is shown inside the control IC in Fig. 1.

Plant transfer functions $G_{PL(A)}$ and $G_{PL(B)}$ of the converter can be written as

$$G_{PL(A)} = A_{OC} \cdot F_M \cdot G_{VD} \tag{20}$$

$$G_{PL(B)} = \frac{G_{PL(A)}}{1+G_{PL(A)}}. \tag{21}$$

Equations (16) and (20) indicate that transfer function $G_{\mathrm{PL}(A)}$ has a pair of complex-conjugate poles near resonant frequency $f_{0A} = \omega_0/(2 \cdot \pi)$. To achieve stability and optimize dynamic performance, the two-zero, three-pole EA compensation is used for the voltage-mode control, i.e.,

$$G_{EA} = \frac{\omega_i \cdot [1+s/\omega_{Z1}] \cdot [1+s/\omega_{Z2}]}{s \cdot [1+s/\omega_{P1}] \cdot [1+s/\omega_{P2}]}. \tag{22}$$

Implementation of transfer function (22) is shown in [11], which also provides relationships between pole/zero frequencies and component values. Asymptotic Bode plots of the plant and EA transfer functions, as well as of loop gain T_A, are shown in Fig. 4 for the compensation design based on loop gain T_A. In this compensation, zero $f_{Z1} = \omega_{Z1}/(2 \cdot \pi)$ is placed at plant A resonant frequency f_{0A} and zero $f_{Z2} = \omega_{Z2}/(2 \cdot \pi)$ is placed between f_{0A} and expected loop crossover frequency f_C. Compensation pole $f_{P1} = \omega_{P1}/(2 \cdot \pi)$ is placed at the ESR zero frequency, and pole $f_{P2} = \omega_{P2}/(2 \cdot \pi)$ is placed between f_{P1} and the switching frequency. Both loop gains T_A and T_{B} have same crossover frequency f_C and expected to have similar stability margins. Since the loop gains cross 0 dB axis with the -1 slope, the phase margin of approximately 90° is expected.

When the EA design is based on loop gain T_{B}, the corresponding asymptotic Bode plots are shown in Fig. 5. Plant B has the resonant frequency $f_{0B} \approx f_{0A} \cdot \sqrt{1+G_{PL(A)}(0)}$ [10]. Compensator zero f_{Z1} is placed between f_{0A} and $f_{0\mathrm{B}}$, whereas compensator zero f_{Z2} is placed around $f_{0\mathrm{B}}$. Observation of loop gain T_A in Fig. 5 indicates the conditional stability since the phase drops to -270° within the loop bandwidth. Generally, the conditionally stable loop becomes unstable when the loop gain is reduced. Conditional stability is particularly unacceptable in the case of the optocoupler feedback since the optocoupler CTR varies significantly with temperature variations and with aging. It should be noted that loop gain T_{B} shows no sign of the conditional stability since it does not expose the low-frequency dynamics of the power supply. The conditional stability can be avoided if compensator zero f_{Z1} is placed below resonant frequency f_{0A} of plant A. Then, loop gain T_A has -2 slope in

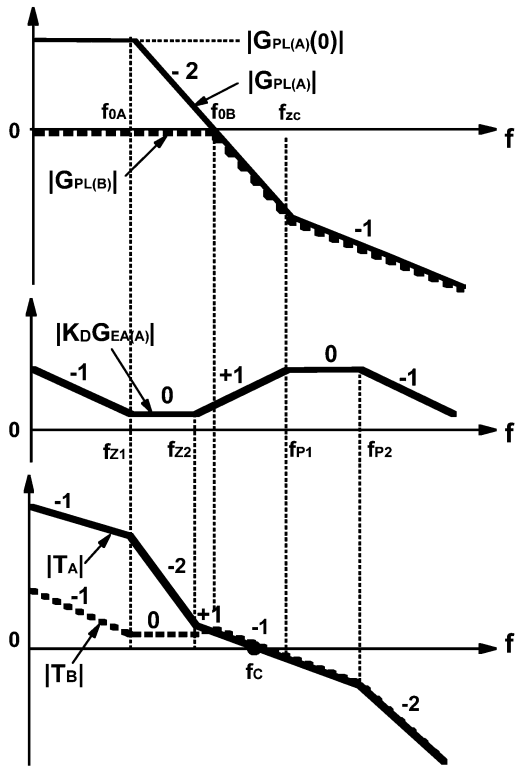

Fig. 4. EA design based on loop gain T_A for voltage-mode control.

the frequency range between f_{0A} and $f_{0\mathrm{B}}$, and T_A phase characteristic does not go below $-180°$.

B. Power Supplies With Current-Mode Control

In the case of the current-mode control, the ramp signal for the PWM in Fig. 1 is derived by sensing the current through filter inductor L_F. It should be noted that in practice the sensing of the inductor current is replaced with the sensing of the primary switch current. Simplified control-to-output transfer function of the forward converter with the current-mode control is given by [12]

$$G_{PL(A)} = A_{OC} \cdot G_{VC} = A_{OC} \cdot \frac{R_L}{R_S} \cdot \frac{1 + s/\omega_{ZC}}{1 + s/\omega_{PA}} \tag{23}$$

where frequencies of poles and zeroes are

$$\omega_{ZC} = 1/(R_C \cdot C_F) \tag{24}$$

$$\omega_{PA} = 1/[(R_L + R_C) \cdot C_F] \tag{25}$$

and R_{S} is the current-sensing gain.

The asymptotic Bode plots of the plant transfer functions $G_{PL(A)}$ and $G_{PL(B)}$ are shown in Fig. 6. Plant B has higher pole frequency $f_{0\mathrm{B}}$ than that of plant A which is governed by equation

$$f_{PB} \approx f_{PA} \cdot G_{PL(A)}(0). \tag{26}$$

As can be seen in Fig. 6, $G_{PL(B)}$ magnitude stays close to unity in the frequency range below f_{PB}. Therefore, the transfer function of plant B does not reveal the low-frequency dynamic characteristics of the power stage. Fig. 6 also shows the asymptotic Bode plot of the compensation network for plant A with one zero and two poles

$$1 + K_D \cdot G_{EA} \approx K_D \cdot G_{EA} = \frac{\omega_i \cdot [1 + s/\omega_{Z1}]}{s \cdot [1 + s/\omega_{P1}]} \tag{27}$$

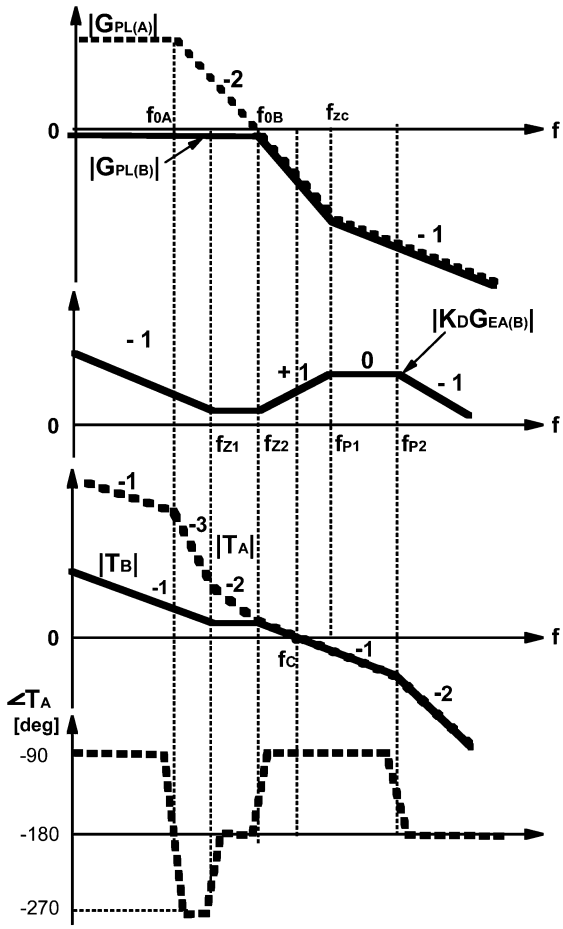

Fig. 5. EA design based on loop gain T_{B} for voltage-mode control.

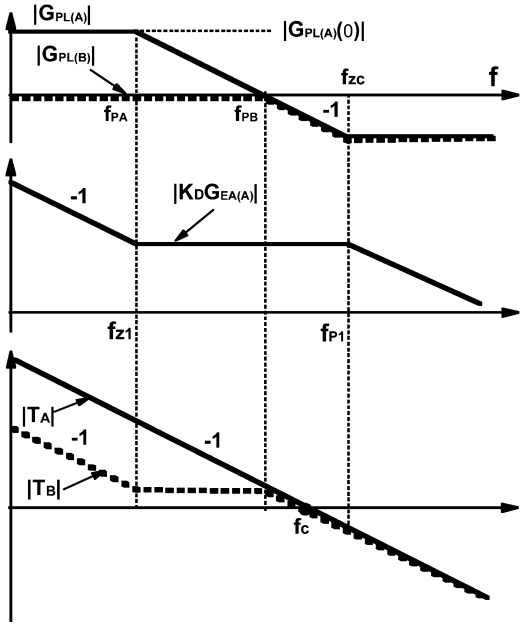

Fig. 6. EA design based on loop gain T_A for current-mode control.

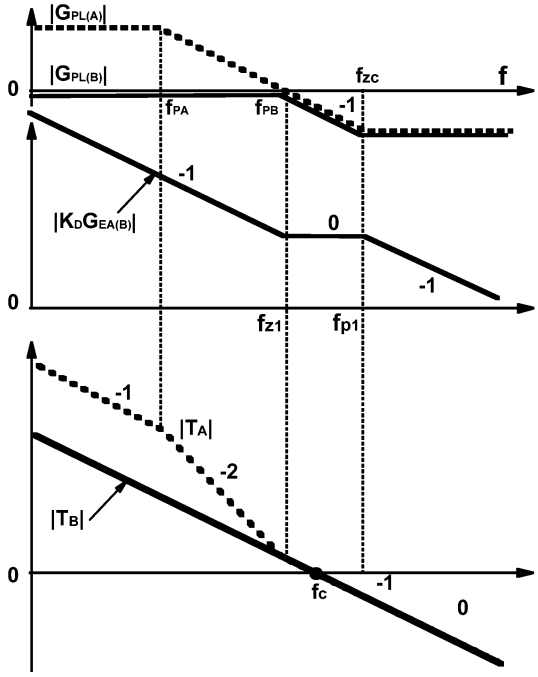

Fig. 7. EA design based on loop gain $T_{\rm B}$ for current-mode control.

which is typically used in converters with the current-mode control. The compensation zero f_{Z1} is placed at pole $f_{\rm PA}$ frequency, and compensation pole f_{P1} is placed at $f_{\rm ZC}$ zero frequency. The resulting asymptotic Bode plots of loop gains T_A and $T_{\rm B}$ in Fig. 6 have same crossover frequency f_C and expected to have similar ample stability margins.

When the error amplifier design is based on loop gain $T_{\rm B}$, the corresponding asymptotic Bode plots are shown in Fig. 7. Compensation zero f_{Z1} and pole $f_{\rm P1}$ are placed to coincide with pole $f_{\rm PB}$ and zero $f_{\rm ZC}$, respectively. As Fig. 7 demonstrates, crossover frequencies and predicted phase margins are essentially the same for loop gains T_A and $T_{\rm B}$. Since the loop gains cross the 0 dB axis with the -1 slope, the phase margin is expected to be close to 90°.

C. TL431 Frequency Response Limitations

In the preceding analysis, it was assumed that EA transfer function $G_{\rm EA}$ is completely determined by compensation networks Z_{C1} and Z_{C2} in Fig. 1, namely

$$G_{EA} = Z_{C2}/Z_{C1}. \tag{28}$$

This assumption is valid only when the EA has the infinite gain in the frequency range of interest. If the TL431 finite gain-bandwidth product is accounted, the EA transfer function can be derived as

$$G_{EA} = \frac{Z_{C2}}{Z_{C1}} \cdot \frac{1}{1+(1+Z_{C2}/Z_{C1})/A_O}, \tag{29}$$

where $A_O(s)$ is the TL431 open-loop gain. If $A_O(s)$ characteristics were well defined, the last equation would provide for an accurate EA design. Unfortunately, the information about the TL431 open-loop frequency response, available from the manufacturer data sheets, is very sketchy and insufficient for the accurate EA design. In addition, the TL431 frequency response

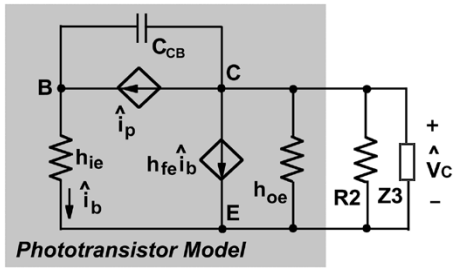

Fig. 8. Small-signal model of the optocoupler circuit.

strongly depends on the regulator dc cathode current and values of the components connected to its output, namely, R_1 and Z_{C2}. Nevertheless, based on the authors' practical experience, several practical observations can be made.

First, for EA transfer function $G_{\rm EA}$ to be completely determined by (28), relationship

$$|G_{EA}| \ll |A_O| \tag{30}$$

must be met. Inequality (30) is practically met if its left side is less than its right side by 30–40 dB. If (30) is violated, but still $|G_{EA}| < |A_O|$, then (29) can be used with the typical values of 50–60 dB dc gain and 0.7–1.0 MHz bandwidth. The TL431 certainly cannot implement the EA transfer function whose gain is above the shunt regulator open loop gain.

Second, as in the case of an operational amplifier, the large capacitance connected to the TL431 output severely limits the regulator bandwidth. Therefore, compensation network Z_{C2} should be implemented with the minimum capacitance amount. Namely, the value of the capacitor between the TL431 cathode and reference pins should not exceed several hundred pF.

D. Optocoupler Circuit Small-Signal Model

The dynamic model of the isolated power supply is incomplete without considering the small-signal characteristics of the optocoupler. The optocoupler small-signal model [13], corresponding to the circuit in Fig. 1, is shown in Fig. 8. The circuit in Fig. 8 contains the bipolar transistor hybrid model in the common-emitter configuration with following parameters: h_{ie}—input resistance with shorted output, h_{oe}—output conductance with open input, h_{fe}—forward amplification gain. The phototransistor model in Fig. 8 also includes collector-base junction capacitance C_{CB} and two dependent current sources $\hat{i}_P = \hat{i}_F \cdot CTR/h_{fe}$ and $h_{fe} \cdot \hat{i}_B$. Since the collector-base junction in phototransistors is used as a light detector, its area is relatively large. As a result, phototransistors have high capacitance C_{CB} that limits their bandwidth. The typical values of the optocoupler parameters used in the power supplies are $C_{CB} = 15$ pF and $h_{FE} = 350$. Using the diagram in Fig. 8 and assuming $\hat{V}_{BE} \ll \hat{V}_{CE}, 1/h_{OE} \gg R_2 \,||\, Z_{C3}$, the optocoupler circuit transfer function is derived

$$A_{OC} = \frac{CTR}{R_1} \cdot \frac{1}{1/(R_2 \,||\, Z_{C3}) + s \cdot C_{CB} \cdot h_{FE}}. \tag{31}$$

When network Z_{C3} consists of single capacitor C_2, (31) is simplified to

$$A_{OC} = CTR \cdot \frac{R_2}{R_1} \cdot \frac{1}{1+s/\omega_{OC}} \tag{32}$$

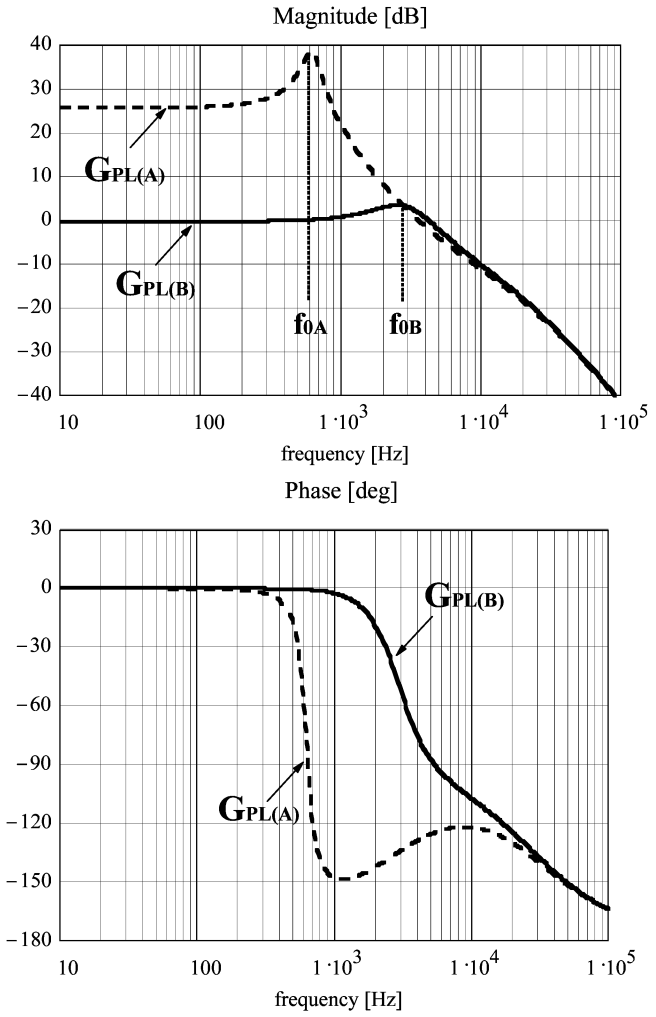

Fig. 9. Transfer functions of plants A and B for voltage-mode control.

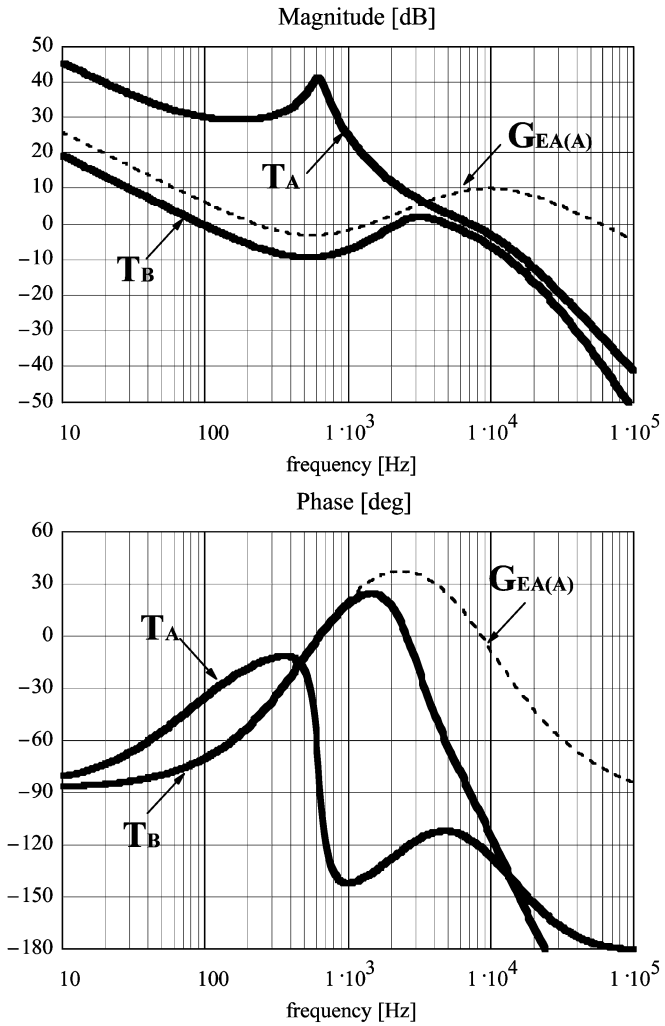

Fig. 10. Loop gain design based on plant A for voltage-mode control.

where

$$\omega_{OC} = 1/[R_2 \cdot (C_2 + h_{FE} \cdot C_{CB})]. \tag{33}$$

It should be noted that the maximum value of pole frequency ω_{OC} is limited by the phototransistor parameters C_{CB} and h_{FE}. For example, for $R2 = 1$ kΩ the frequency of this pole is below 30 kHz.

IV. Design Example

This section considers the 380-V/5-V, 20-A, 100-kHz forward power supply, whose simplified schematic is shown in Fig. 1. Transformer with turns ratio N of 20:1 is assumed. The output filter inductor value is $L_F = 10$ μH, whereas output capacitance consists of two 3300-μF aluminum capacitors with 18-mΩ ESR each. The design example also assumes modulator gain $F_{\rm M} = 1$ V^{-1} and the optocoupler circuit values of CTR $= 100\%$ and $R_1 = R_2 = 1$ kΩ.

The Bode plots of the plant and EA transfer functions, as well as the Bode plots of loop gain T_A, are shown in Fig. 10. The EA compensation with $\omega_{\rm i} = 1.2 \cdot 10^3$ rad/s, $f_{Z1} = f_{Z2} = 550$ Hz, $f_{\rm P1} = f_{\rm P2} = 10$ kHz was chosen to provide 7.1-kHz T_A bandwidth with the corresponding phase margin of 63°. As can be seen from Fig. 10, for this EA compensation, loop gain $T_{\rm B}$ has only 90-Hz bandwidth and corresponding 105° phase margin. This implies that a wide bandwidth of T_A does not translate into a wide bandwidth of $T_{\rm B}$.

A. Power Supply With Voltage Mode Control

The Bode plots of plant transfer functions $G_{{\rm PL}(A)}$ and $G_{{\rm PL(B)}}$ of the power supply with the voltage-mode control are shown in Fig. 9. The plant transfer functions in Fig. 9 are different at low frequencies where $A_{\rm OC} \cdot G_{\rm VC} \gg 1$. Actually, due to the inner loop influence, plant transfer function $G_{PL(B)}$ does not expose the control loop dynamics at low frequencies where its value is close to unity. Also between resonant frequencies $f_{0A} = 0.6$ kHz and $f_{0B} = 2.8$ kHz, the phase lag of $G_{PL(A)}$ is considerably higher than that of $G_{PL(B)}$. The plots in Fig. 9 indicate that it is much easier to design the EA for plant B than for plant A. The next step is to compare EA designs based on loop gains T_A and $T_{\rm B}$.

Error Amplifier Design Based on Loop Gain T_A:

Error Amplifier Design Based on Loop Gain $T_{\rm B}$: The Bode plots of the plant and EA transfer functions, as well as of the loop gain $T_{\rm B}$, are shown in Fig. 11. The EA compensation with $\omega_{\rm i} = 40 \cdot 10^3$ rad/s, $f_{Z1} = f_{Z2} = 2$ kHz, $f_{\rm P1} = 2.6$ kHz, and $f_{\rm P2} = 40$ kHz was selected to provide 6.9-kHz $T_{\rm B}$ bandwidth

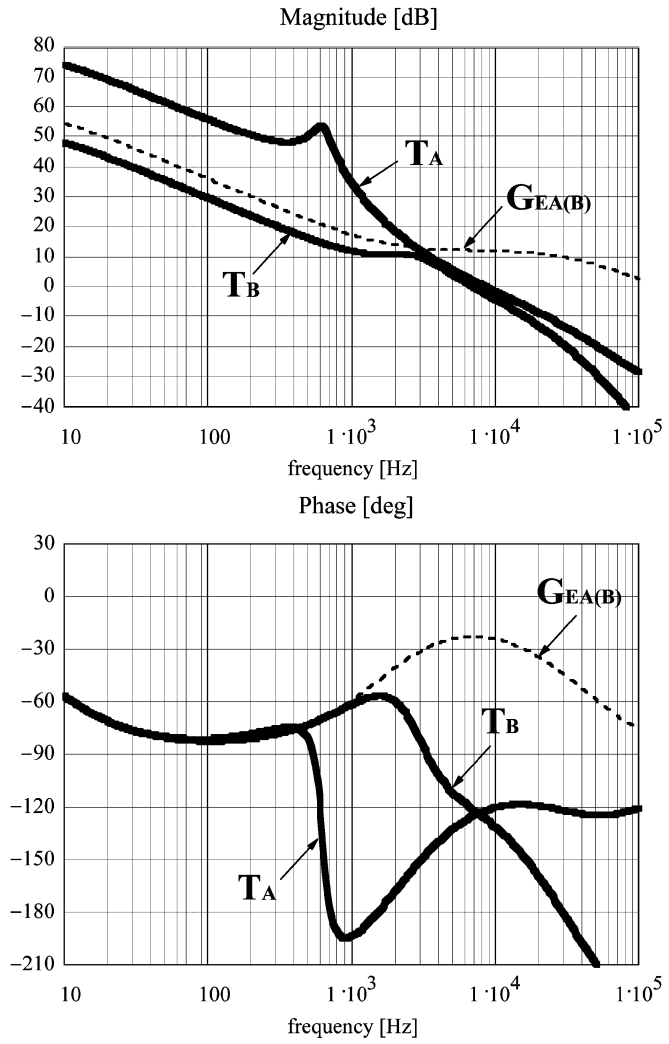

Fig. 11. Loop gain design based on plant B for voltage-mode control.

with the corresponding phase margin of 58°. Fig. 11 also shows loop gain T_A for the EA design mentioned above. The Bode plots in Fig. 11 indicate T_A bandwidth of 7.2 kHz and the phase margin of 55°.

Fig. 11 also shows that loop gain T_A is conditionally stable since its phase drops below $-180°$ around 1-kHz frequency which is within the bandwidth of T_A. The conditional stability is more pronounced at higher Q values of the power stage transfer function. Generally, the conditional stability is not acceptable since the power supply can become unstable during large-signal line transients or as a result of component degradation. Loop gain $T_{\rm B}$ in Fig. 11 does not show the conditional stability problem because the power stage characteristics are hidden within $T_{\rm INNER}$ bandwidth and $G_{\rm PL(B)}$ is not proportional to such critical gains of the inner loop, as the input voltage and the optocoupler CTR. Therefore, the EA design based on loop gain T_A is preferable to the one based on loop gain $T_{\rm B}$.

B. Power Supply With Current-Mode Control

Fig. 12 shows the detailed small-signal block diagram of the converter with the current-mode control. The diagram contains the internal current control loop with following blocks:

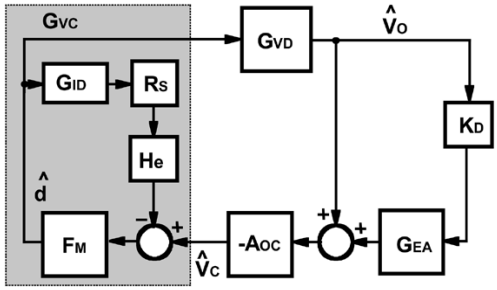

Fig. 12. Small-signal block diagram of isolated power supply with current-mode control.

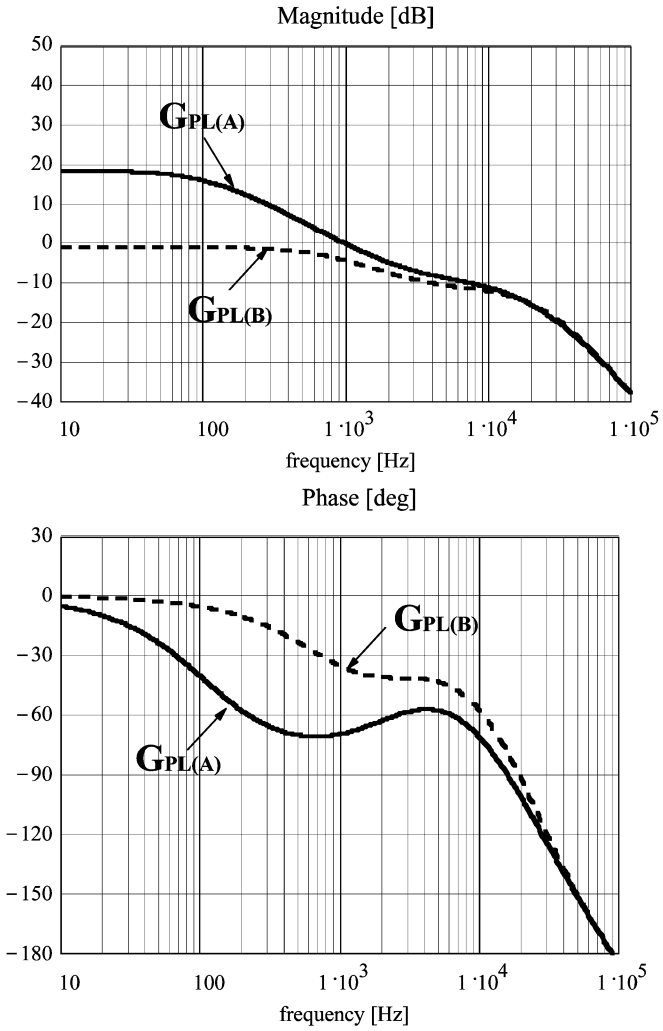

Fig. 13. Transfer functions of plants A and B for current-mode control.

$G_{\rm ID} = \hat{i}_L/\hat{d}$—duty-ratio-to-inductor-current transfer function, H_E—sampling transfer function [14], R_S—current sensing gain, F_M—PWM gain. The parameter values assumed for the current-mode control are $F_{\rm M} = 2.86\ {\rm V}^{-1}$ and $R_{\rm S} = 25\ {\rm m}\Omega$. Based on the diagram in Fig. 12, the control-to-output transfer function is described by equation

$$G_{VC} = \frac{F_M \cdot G_{VD}}{1 + F_M \cdot G_{ID} \cdot R_S \cdot H_E}. \tag{34}$$

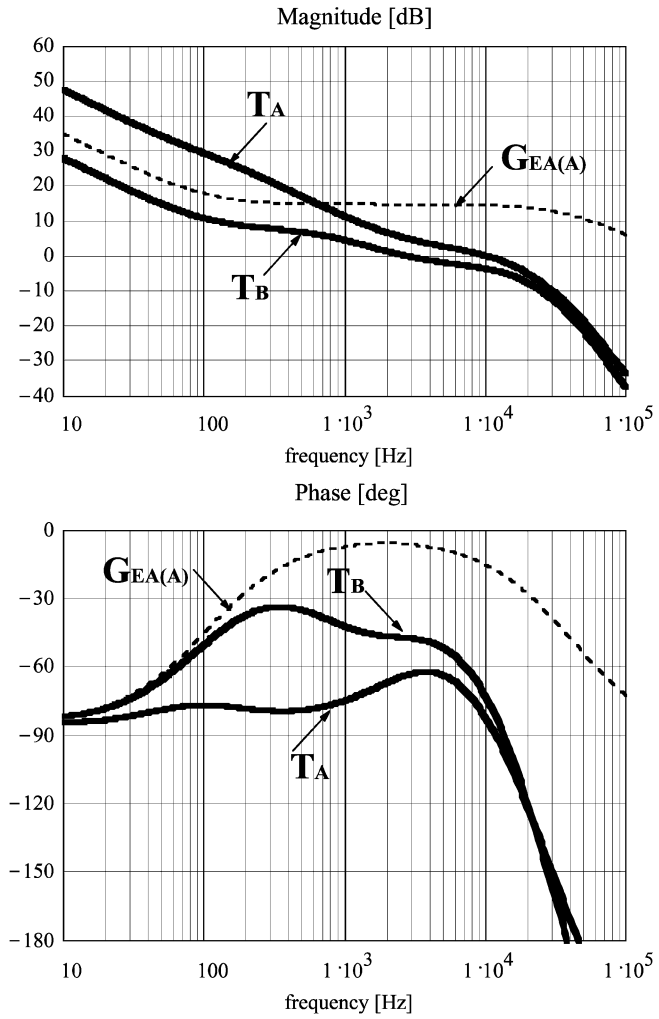

Fig. 14. Loop gain design based on plant A for current-mode control.

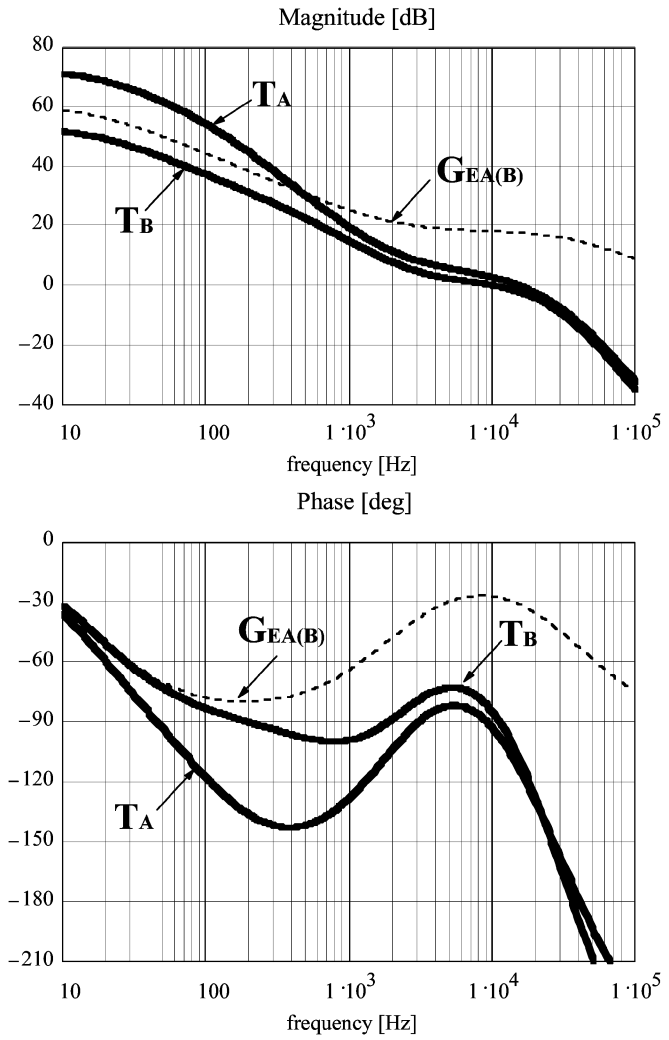

Fig. 15. Loop gain design based on plant B for current-mode control.

Transfer function G_{ID} in (34) is derived based on the PWM switch model [15]

$$G_{ID} = \frac{V_{IN}}{N \cdot R_L} \cdot \frac{1 + s/\omega_{ZD}}{1 + s/(\omega_0 \cdot Q) + s^2/\omega_0^2} \tag{35}$$

where $\omega_{ZD} = 1/(R_L \cdot C_F)$, ω_0 and Q are defined by (17) and (18).

The Bode plots of plant transfer functions $G_{\mathrm{PL}(A)}$ and $G_{\mathrm{PL(B)}}$ are shown in Fig. 13. As Fig. 13 demonstrates, the plant transfer functions are different at low frequencies where $A_{\mathrm{OC}} \cdot G_{\mathrm{VC}} \gg 1$. Actually, due to the inner loop influence, the plant B phase characteristic exhibits less phase lag at low frequencies and, therefore, loop gain T_{B} is easier to compensate than loop gain T_A. The next step is to compare EA designs based on loop gains T_A and T_{B}.

Error Amplifier Design Based on Loop Gain T_A: Fig. 14 shows the loop gain design for plant A which produces following locations of compensator poles and zeroes: $\omega_{\mathrm{i}} = 3.45 \cdot 10^3$ rad/s, $f_{Z1} = 100$ Hz, and $f_{\mathrm{P1}} = 50$ kHz. This design provides 10-kHz loop bandwidth with the corresponding phase margin of 97°. Fig. 14 also shows loop gain T_{B} corresponding to the compensator design for plant A. The loop gain T_{B} has 2.7-kHz loop bandwidth with the corresponding phase margin of 133°.

Error Amplifier Design Based on Loop Gain T_{B}: The corresponding EA transfer function and loop gain T_{B} are plotted in Fig. 15. The compensator has following poles and zeroes: $\omega_{\mathrm{i}} = 105 \cdot 10^3$ rad/s, $f_{Z1} = 2$ kHz, and $f_{\mathrm{p1}} = 50$ kHz. This design provides 10-kHz loop bandwidth for loop gain T_{B}, the same as the bandwidth for loop gain T_A in the case when the design was done for plant A. The phase margin of loop gain T_{B} is 95°. Fig. 15 also shows loop gain T_A corresponding to the compensator design for plant B. The loop gain T_A has 15-kHz loop bandwidth with the phase margin of 68°.

Observation of Figs. 9–11 and Figs. 13–15 indicates that the magnitude of loop gain T_A is higher than that of loop gain T_{B}. $|T_A|$ is higher than $|T_{\mathrm{B}}|$ at low frequencies since $|G_{\mathrm{PL}(A)}|$ is higher than $|G_{\mathrm{PL(B)}}|$ at low frequencies. $|T_A|$ is higher than $|T_{\mathrm{B}}|$ at high frequencies since $|1 + K_{\mathrm{D}} \cdot G_{EA}|$ is higher than $|K_{\mathrm{D}} \cdot G_{EA}|$ at high frequencies. At the same time, the phase lag of loop gain T_A is generally higher than that of loop gain T_{B}. Therefore, if the EA design is based on loop gain T_A, loop gain T_{B} is expected to have lower bandwidth and higher stability margins than loop gain T_A.

The presented design example implies that, in the case of the current-mode control, both loop gains T_A and T_{B} can be used for the EA design.

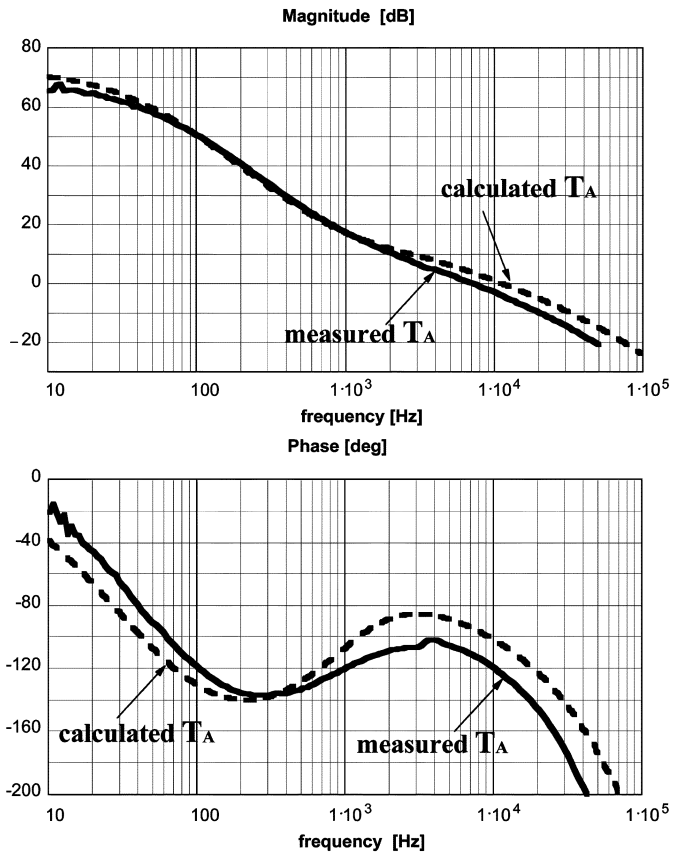

Fig. 16. Measured loop gain corresponding to breaking the loop at point A.

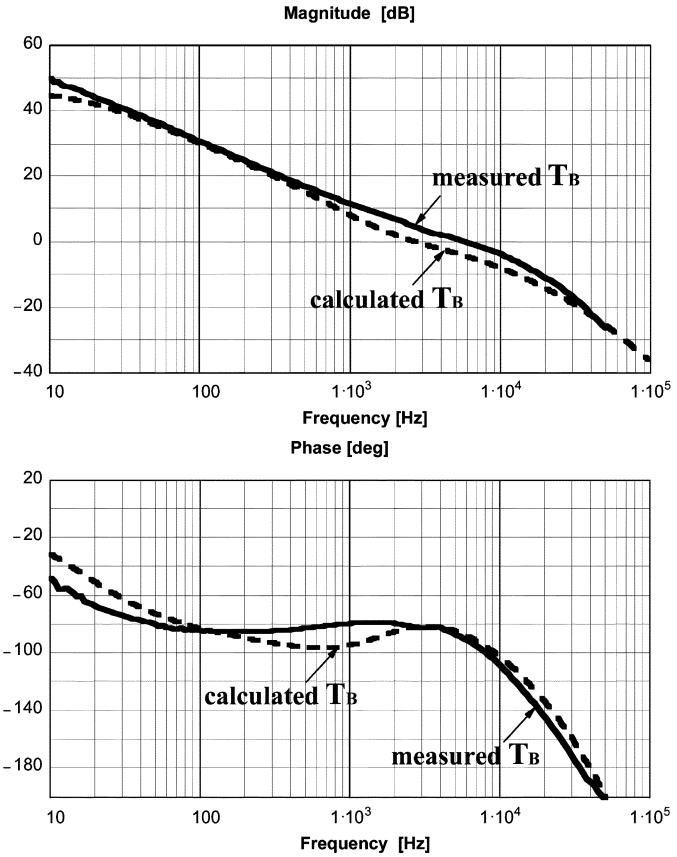

Fig. 17. Measured loop gain corresponding to breaking the loop at point B.

V. Experimental Results

The 380-V/12-V, 45-A two-switch forward power supply operating at 100-kHz switching frequency is used as an experimental prototype. The power transformer has $N = 10{:}1$ turns ratio. The output filter inductor value is $L_F = 11.5$ uH. Output capacitance C_F is implemented with three 3300-uF aluminum capacitors each having 35-mΩ ESR. The converter operates with current-mode control that is implemented by sensing the primary switch current with 0.15-Ω resistor. Compensation network Z_{C2} is a series connection of a 27-kΩ resistor and a 5.6-nF capacitor, whereas network Z_{C1} is a short circuit. Resistors of output voltage divider have values $R_{D1} = 7.6$ KΩ and $R_{D2} = 2$KΩ. Therefore, the EA transfer function has a single pole at the origin and one zero at 1-kHz frequency. The second compensation pole is introduced by network Z_{C3} on the primary side. The prototype employs SFH617A-3 optocoupler with the CTR range of 100–200%, $C_{\rm CB} = 6$ pF, and $h_{\rm FE} = 250$. The component values of the optocoupler circuit are $R_1 = R_2 = 1$ k$\Omega, C_2 = 4.7$ nF, where C_2 is the sole component of compensation network Z_{C3} in Fig. 1.

Bode plots of the loop gains corresponding to breaking the loop at points A and B are shown in Figs. 16 and 17, respectively. Loop gain T_A has a crossover frequency of 6.7 kHz, a phase margin of 68° and a gain margin of 18 dB, whereas loop gain $T_{\rm B}$ has a bandwidth of 5.6 kHz, a phase margin of 90° and a gain margin of 19 dB. Figs. 16 and 17 demonstrate that loop gains T_A and $T_{\rm B}$ have similar crossover frequencies and stability margins for the optimized compensation and each can be used for the EA design. For analysis verification, Figs. 16 and 17 also show calculated loop gains T_A and $T_{\rm B}$. Measured and calculated loop gains have reasonable agreement with each other.

VI. Conclusion

In the isolated power supplies with the optocoupler feedback, two loops can be identified with corresponding loop gains T_A and $T_{\rm B}$. The comparative analysis shows that loop gain T_A provides more straightforward design approach and more meaningful relationship between the loop gain and converter response to the line and load disturbances. It was found that in power supplies with the current-mode control both loop gains can be used for the compensation design. However, in the power supplies with the voltage-mode control the bandwidth can be very different depending on which loop gain was used for the compensator design. Also, in the power supplies with the voltage-mode control it is preferable to use loop gain T_A for the EA design in order to avoid the conditional stability. Dynamic limitations of the TL431 shunt regulator and of the optocoupler were discussed. Practical guidelines for the compensation design in converters with current-mode and voltage-mode controls, as well as experimental results were presented.

References

[1] B. Mammono, "Isolating the control loop," in *Proc. Unitrode Sem.*, 1997, pp. C-21–C2-15.

[2] *Handbook of Switchmode Power Supplies*, K. Billings, Ed., McGraw-Hill, New York, 1989.

[3] D. Venable. (2005) Stability testing of multiloop converters. *Venable Instruments Reference Tech Papers* [Online]. Available: www.venable.biz/tr-papers2.html
[4] T. H. Chen, "Dynamic modeling and control design of flyback converter," *IEEE Trans. Aerosp. Electron. Syst.*, vol. 35, no. 4, pp. 1230–1239, Oct. 1999.
[5] R. Kollman and J. Betten, "Closing the loop with a popular shunt regulator," *Power Electron. Technol. Mag.*, pp. 30–36, Sep. 2003.
[6] ——, "Compensating the (often missed) inner and outer control loops using the TL431," in *Proc. Power Electronic Technology Conf.*, Rosemont, IL, Oct. 2002, pp. 366–377.
[7] R. Ridley, "Designing with the TL431," *Switching Power Mag.*, vol. 5, no. 2, pp. 20–26, 2004.
[8] R. Stefani, C. Savant, B. Shahian, and G. Hostetter, *Design of Feedback Control Systems*. Philadelphia, PA: Saunders College Publishing, 1994, p. 521.
[9] C. H. Yang, D. Y. Chen, C. Jamerson, and Y. P. Wu, "Stabilizing magamp control loop by using an inner-loop compensation," in *Proc. Applied Power Electronics Conf.*, Mar. 1991, pp. 365–372.
[10] I. J. Lee, D. Y. Chen, C. Jamerson, and Y. P. Wu, "Modeling of control loop behavior of magamp post regulators," in *Proc. Applied Power Electronics Conf.*, Mar. 1991, pp. 365–372.
[11] A. I. Pressman, *Switching Power Supply Design*. New York: McGraw-Hill, 1991, p. 455.
[12] R. W. Erickson and D. Maksimovic, *Fundamentals of Power Electronics*. Norwell, MA: Kluwer, 2001.
[13] J. Bliss, "Theory and characteristics of phototransistors," *Motorola Application Note AN-440, Motorola Databook "Optoelectronics Device Data"*, pp. 9.3–9-13, 1989.
[14] R. B. Ridley, "A new, continuous-time model for current-mode control," in *Proc. Power Conversion Intelligence Motion Conf.*, Long Beach, CA, Oct. 1989, pp. 455–464.
[15] V. Vorperian, "Simplified analysis of PWM converters using the model of the PWM switch part I: Continuous conduction mode," in *Proc. VPEC Sem.*, Blacksburg, VA, Sep. 1989, pp. 1–9.

Yuri Panov received the Dipl.-Eng. and Ph.D. degrees in electrical engineering from the Moscow Aviation Institute, Moscow, Russia, and the M.S.E.E degree from the Virginia Polytechnic Institute and State University, Blacksburg.

He is currently a Senior R&D Staff Member with Delta Products Corporation, Research Triangle Park, NC. His 20-year experience includes dc/ac, ac/dc, and dc/dc power conversion; modeling and design of large-scale power systems for aerospace applications; and design of various analog electronics circuits. His current research is focused on high-power-density offline power supplies and dc–dc converters for next generations of computers.

Milan M. Jovanović (F'01) was born in Belgrade, Serbia. He received the Dipl.-Ing. degree in electrical engineering from the University of Belgrade, Serbia.

Presently, he is the Chief Technology Officer of Delta Electronics, Inc., Taipei, Taiwan, R.O.C., one of the world's largest manufacturers of power supplies.